DEFECTS IN THIN EPITAXIAL LAYERS OF $(Al_xGa_{1-x})_2O_3$ GROWN ON Al_2O_3 SUBSTRATES

A.V. Kremleva[1,2*], D.A. Kirilenko[1,2], V.I. Nikolaev[1,2,4], A.I. Pechnikov[1,4],

S.L. Stepanov[1,4], M.A. Odnoblyudov[3], V.E. Bougrov[1], A.E. Romanov[1,2]

[1]Saint Petersburg National Research University of Information Technologies, Mechanics and Optics,

Kronverskii avenue 49, St. Petersburg, 197101, Russia

[2]Ioffe Institute of the Russian Academy of Sciences, Polytechnicheskaya str. 26, St. Petersburg, 194021, Russia

[3]Peter the Great St. Petersburg Polytechnic University, Polytechnicheskaya str.29, St. Petersburg, 195251, Russia

[4]LLC Perfect Crystals, Polytechnicheskaya str. 26 A, St. Petersburg, 194064, Russia

*e-mail: avkremleva@corp.ifmo.ru

Abstract. Gallium oxide is considered as a perspective functional material for a wide range of applications. This includes light emitting devices, high power electronics, gas sensors and catalysts. Investigation of its structural features, particularly, defect structure of the gallium oxide epitaxial layers is crucial for the high quality devices production technology development. This work is focused on the investigation of the defect structure of thin epitaxial layers of $(Al_xGa_{1-x})_2O_3$ possessing monoclinic structure grown by hydride vapor phase epitaxy on Al_2O_3 substrates. Some of the observed plane defects, twins and stacking faults, are shown for the first time.

Keywords: gallium oxide; twins; stacking faults; dislocations; hydride vapor phase epitaxy; tilted domains; transmission electro microscopy.

1. Introduction

Development of the semiconductor technology is approaching the point where the potential of conventional materials is depleted. In order to overcome the possible stagnation significant efforts have been focused on elaboration of new semiconducting material concepts. In this sphere, the so-called transparent oxide semiconductors (TOS) are considered as a very perspective class of materials, which presents certain advantages over conventional bases of semiconductor technology like Si, SiC, GaAs, sapphire etc. Transparency is the crucial advantage for a variety of light-emitting devices leading to higher standards of efficiency in energy-saving applications. Transparent oxides are highly chemically inert and yet chemically sensitive which enables their diverse application in chemical sensors for harsh environments. Descent electrical conductivity of these materials makes them a preeminent substitute for insulating substrates, and, thus, allows to produce electronic devices with vertical chip design. Transparent semiconductors, being a wide-gap material, are well suited for high power applications. A prominent representative from this class is gallium oxide – it can be employed in most of the above-mentioned fields.

This material, especially the monoclinic phase β-Ga_2O_3, which is the most stable form at ambient conditions has been studied from a view point of possible applications [1]. Gallium oxide can be implemented as a rare-earth phosphor host for electroluminescent devices and displays because tri-valent rare earth species are isovalent to Ga(III) cations in the gallium oxide

structure. This property combined with high transparency and chemical stability allows to produce efficient phosphors of wide spectral range [2-4]. Transparent and conductive gallium oxide substrates can be employed in light emitting devices based on III-nitride technology. High brightness InGaN diodes grown on β-Ga_2O_3 substrates have been demonstrated [5]. Shottky diodes with outstanding characteristics have been produce using various metal contacts [6-8]. Gallium oxide nanowires have shown high performance of field emission [9]. β-Ga_2O_3 can be used for sensing hydrogen [10], oxygen [11] and various organic vapors [12]. Gallium oxide possesses high catalytic activity in dehydrogenation and oxidation of hydrocarbons [13,14] and photoelectrolysis of water [15] due to unique structural characteristics of coordinatively unsaturated surface Ga^{3+} cations. Additionally, β-Ga_2O_3 has a significantly higher critical electric field value and Baliga's figure of merit (FOM) [16] compared to those for SiC or sapphire, which beneficial for applications in high-power devices [17].

The interest provoked by possible technological applications of gallium oxide has stimulated fundamental studies of electronic, structural and other basic properties of the material. Significant progress has been made to date; however, many uncertainties and unexplained phenomena remain are yet to be explored as it can be seen in literature sources (e.g. in the reviews [18-21]). Structural properties of monoclinic gallium oxide phase (β-Ga_2O_3) are also non-trivial due to complexity of the structure itself and can exhibit unpredicted behavior, especially, in the case of gallium oxide nanostructures. For this reason, we present a study of plane defects found in epitaxial layers of $(Al_xGa_{1-x})_2O_3$ grown on sapphire substrates. Besides the defects, described in the literature (e.g. [22-30]), we observed certain defects, which might be specific for the gallium oxide grown on sapphire. The focus of the study lies on the possible orientational relationships between various gallium oxide grains and between the grains and the substrate. The observed twins and stacking faults may point to some new ways in epitaxial structures engineering and provide a better understanding of the structural and mechanical properties of the material.

2. Experimental

Epitaxial layers $(Al_xGa_{1-x})_2O_3$ were grown on *c*-plane sapphire substrates in a home-made hot wall atmospheric pressure HVPE reactor. The reactor consisted of a 75 mm quartz tube placed in a multi zone horizontal furnace. GaCl and dry air were used as precursors. The air was produced by liquefaction and evaporation of atmospheric air and therefore consisted mainly of 21 % of oxygen, 78 % of nitrogen, 1 % of argon and other noble gases. Impurities such as moisture, carbon dioxide, hydrocarbons, etc. were present only in trace amounts (ppm range). The GaCl vapor was synthesized *in-situ* upstream in the reactor by the reaction of metallic gallium (99.9999%) and gaseous hydrogen chloride (99.999 %) at 600 °C. The yield of GaCl formation was estimated to be over 80 %. Similarly to that $AlCl_3$ vapor was synthesized by reaction of HCl stream with Al. Then the precursor vapors was transported to the deposition zone of the reactor held at 1050 °C where it was mixed with air to produce $(Al_xGa_{1-x})_2O_3$. The HCl flow through the source was varied from 100 sccm to 400 sccm. The maximal HCl flow was limited by the range of the mass flow controller used, so higher flow were not investigated. The air flow was kept constant at 4 slm. Argon was used as a carrier gas and the total gas flow through the reactor was 10 slm. The input VI/III ratio was in the range from 2 to 8. Under these conditions the deposition rate was in the range from 70 to 250 mm/ h. The deposition time was adjusted accordingly to obtain $(Al_xGa_{1-x})_2O_3$ layers with the thickness in the range of 0.5–1 mm. After the growth the substrate was cooled down to room temperature under argon flow.

The structure of $(Al_xGa_{1-x})_2O_3$ layers was analysed by means of transmission electron microscopy (TEM). For this purpose cross-sectional TEM specimens were prepared by a conventional procedure comprising face-to-face gluing of the wafer pieces, mechanical grinding and polishing down to the thickness of about 10-20 µm and subsequent ion milling

using Ar^+ beam at 4 keV. Areas of the specimen, which were sufficiently transparent for high-energy electrons (i.e. less than about 100 nm in thickness), were studied and the defect structure of the epitaxial layers was analysed using Jeol JEM-2100F transmission electron microscope (accelerating voltage 200 kV, point-to-point resolution 0.19 nm). Conventional selected area electron diffraction (SAED) technique was used for analysis of the crystal structure and orientational relationships. Conventional dark-field (DF) imaging was used for the visualization of crystal grains, grain boundaries and for the analysis of plane defects in gallium oxide.

3. Results and Discussion

3.1 Twinning on the plane (100). This type of twinning in gallium oxide grown on *c*-plane oriented sapphire is often observed because (100) plane is a cleavage plane in this structure and stacking fault formation energy is quite low on this plane. For this reason, twin boundaries usually coincide with the twinning plane; an example of such structure with multiple (100) twins is presented in Fig. 1. It is well seen in these images that twin boundaries are mostly parallel to (100) planes. However, some of the boundaries are obviously inclined to this system of planes and are almost parallel either to (001) or (001)* planes (here and further the asterisk sign denotes crystallographic objects of the twinned part of the crystal) which actually coincide with $(\bar{2}02)^*$ or $(\bar{2}02)$ respectively.
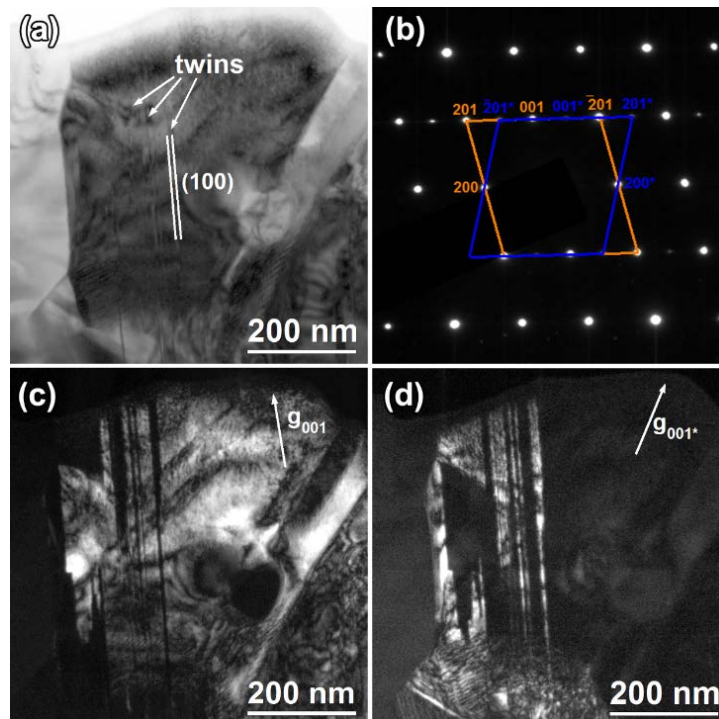

Fig. 1. (100) twins in epitaxial $(Al_xGa_{1-x})_2O_3$ layer grown on sapphire substrate (0001). (a) Bright-field image showing a grain with multiple (100) twins. (b) Electron diffraction pattern with two subsets of diffraction spots related to the original and twinned crystal lattices. (c) Dark-field image obtained using (001) spot of original lattice. (d) Dark-field image obtained using (001)* spot of the twinned structure so that only twins are visible.

TEM images for *m*-plane $(Al_xGa_{1-x})_2O_3$ epitaxial layer grown on *c*-plane oriented sapphire present another evidence for the presence of twin boundaries non-parallel to the (100) twinning plane. Fig. 2 shows an example of such structure with multiple twinning on the (100) plane similar to the described above. However, in this case the diffraction pattern (Fig. 2a) shows a set of forbidden diffraction spots which arise due to double-diffraction. This, in turn, is possible if twin and parent crystals are both in the way of the electron beam, which is perpendicular to

the TEM image plane. Therefore the twin boundary is inclined to the electron beam which is parallel to the [010] direction in the presented images. Thus the twin boundary cannot be (100) plane or any other plane from the [010] zone axis. Also, dark-field images (Fig. 2b and Fig. 2c) showing twinned and original crystal parts show that some areas introduce bright contrast in both images. Additionally, the presence of the crystal and its twin above each other in such projection produces Moiré patterns (Fig. 2d), which usually arise because of superposition of two lattice images.

Fig. 2. Example of multiple (100) twins in epitaxial $(Al_xGa_{1-x})_2O_3$ layer grown on sapphire substrate (0001). (a) Electron diffraction pattern with two subsets of diffraction spots, the systematic raw {1+2n 0 0} related to double diffraction is visible. (b) and (c) Dark-field images of the structure. Arrows indicate areas of bright contrast in both images where twin boundary is inclined to the image plane. (d) High-resolution TEM image of the $(Al_xGa_{1-x})_2O_3$ lattice showing Moiré pattern produced by superposition of diffraction patterns from twin domains.

The (100) plane is a cleavage plane of monoclinic gallium oxide, and thus energy of plane defect formation along this plane is relatively low. Such defects can be generated during the cooling of the structure after growth due to mechanical stress caused by the difference of the thermal expansion coefficients of the layer and the substrate. However, we also observed twin boundaries which were inclined to the (100) twinning plane. It is very unlikely that these anomalous twin boundaries resulted from thermal mechanical stresses because this scenario is energetically unfavorable. Alternatively, twining can occur during the very process of epitaxial growth and the observed anomalous twin boundaries are formed by crystal grains growing over each other. This kind of defects can be potentially eliminated by careful optimization of the growth parameters, especially for the initial stage of growth.

3.2 Stacking faults in (111) plane. Another type of defects which we found in these structures are stacking faults on (111) plane (Fig. 3). Stacking faults provide specific contrast in a dark-field image (e.g., Fig. 3b) if the scalar product of their fault vector **R** with the diffraction vector **g** used for this image is non-zero or non-integer. For this reason the stacking faults are almost invisible for certain diffraction vectors used (Fig. 3c and Fig. 3d).

The presented dependence of the stacking fault visibility on diffraction vector allows us to suppose that the fault vector **R** lays in the stacking fault plane thus the stacking faults can result from mechanical stress. In order to determine the stacking fault plane more precisely we tilted the specimen to another zone axii and found that the stacking faults visible as narrow lines when [010] direction is parallel to the electron beam. That is their plane is perpendicular to the image plane in this case.
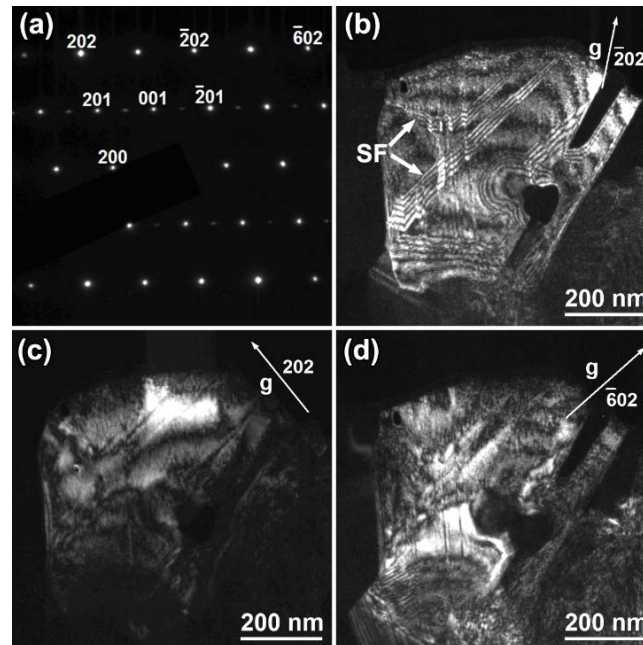

Fig. 3. Stacking fault in $(Al_xGa_{1-x})_2O_3$ layer grown on sapphire substrate (0001). (a) Electron diffraction pattern where the used diffraction spots are marked. (b) Dark-field image obtained using $\bar{2}02$ spot. The stacking faults (SF) are clearly visible. The zigzag shape of the stacking fault is caused by its propagation through a set of twins on (100) plane, so that the direction of the stacking fault plane changes inside twinned part of the crystal lattice. (c) and (d) Dark-field images obtained using $\bar{6}02$ and 202 spots, which are almost perpendicular to each other. The stacking fault in these cases is practically invisible.
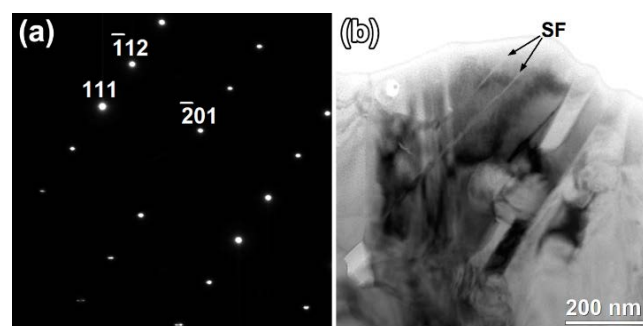

Fig. 4. The observed stacking faults at crystal orientation by $[1\bar{3}2]$ zone axis in $(Al_xGa_{1-x})_2O_3$ on *c*-plane sapphire. (a) Electron diffraction pattern. (b) Image of the stacking faults which are visible as narrow lines because their plane is almost parallel to the electron beam.

According to the relation between stacking fault image and diffraction spots in the diffraction pattern (Fig. 4) we deduced that the observed stacking faults are on (111) plane. It is remarkable, that the stacking fault continuously extends through the (100) twins in the grain and its zig-zag shape (Fig. 3b) corresponds to the different orientation of (111) planes in the twins.

3.3. Growth plane change due to the twinning on $(\bar{1}12)$ plane. Another type of plane defects has been revealed. Fig. 5 presents TEM images of a $(Al_xGa_{1-x})_2O_3$ layer grown on a *c*-plane oriented sapphire substrate. Some of the $(Al_xGa_{1-x})_2O_3$ grains has typical orientation so that $(\bar{2}01)$ plane is parallel to the substrate surface, while their [010] or [132] direction oriented along $[1\bar{1}00]$ axis of sapphire [31]. However, some of the grains have another orientation as can be seen in the electron diffraction pattern presented in Fig. 3a. Analysis of the diffraction spots location shows that it corresponds to the presence of a twin on $(\bar{1}12)$ plane. So, the planes $(\bar{1}12)$ in the twinned and untwinned lattices coincide. The twin boundary parallel to this plane in the presented case.
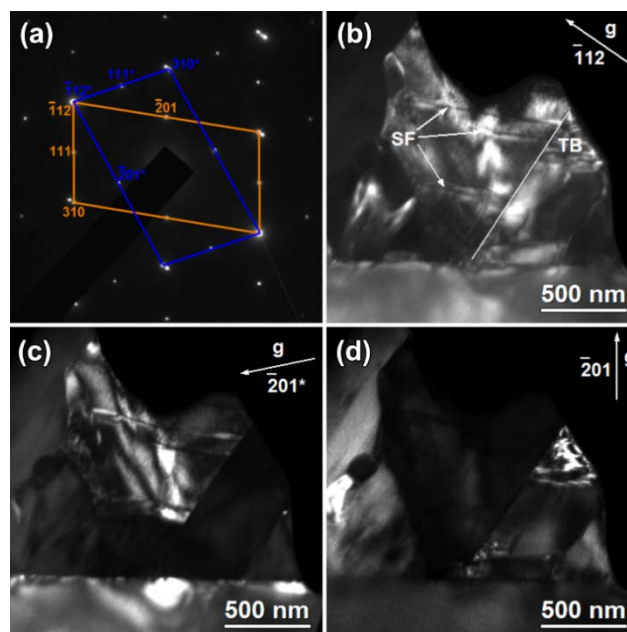

Fig. 5. Twin on the $(\bar{1}12)$ plane in epitaxial $(Al_xGa_{1-x})_2O_3$ layer grown on sapphire substrate (0001). (a) Electron diffraction pattern with the two subsets of diffraction spots. (b) Dark-field image obtained using $\bar{1}12$ spot that corresponds to the twinning plane. The grains are separated by the twin boundary (TB) parallel to $(\bar{1}12)$ plane are visible. (c) and (d) Dark-field images obtained using dedicated $\bar{2}01$ spots of the twin and basic grain. Note, that stacking faults (SF) in (310) plane are visible in the twin.

3.4. Tilted domains. Domains which differ from the rest of the layer by their crystal lattice tilt of about 2-3° have been discovered in the studied samples. The presence of the tilt and its magnitude are determined using electron diffraction patterns (Fig. 6a). In the case of tilt, the shape of diffraction spots changes to elongated streaks. The dark-field images obtained using left and right parts of a streak (Fig. 6b and Fig. 6c) show the shape of the domain tilted respectively to the main part of the layer.

The domains has characteristic size of about several micrometers and consist of various crystalline grains similar to the whole epitaxial film grown on the sapphire substrate. That is the grains in the tilted domain possess the same orientation relationships as described before. However, all the grains, thus, tilted by small angle with respect to the layer and the substrate. The observed domains were overgrown by the main layer structure and, thus, did not affect the orientation of the layer surface. It is worth noting, that the tilted domains were found only in $(Al_xGa_{1-x})_2O_3$ layers thicker than 1 µm.

4. Conclusions
We present a set of plane defects emerging in $(Al_xGa_{1-x})_2O_3$ grown on sapphire substrates. The observed features of the defect structure provide a new insight into the material structural

properties. The fact of twinning on the plane ($\bar{1}12$), which transforms the growth plane into (310), may be useful for better control of the growth modes and epitaxial design development.
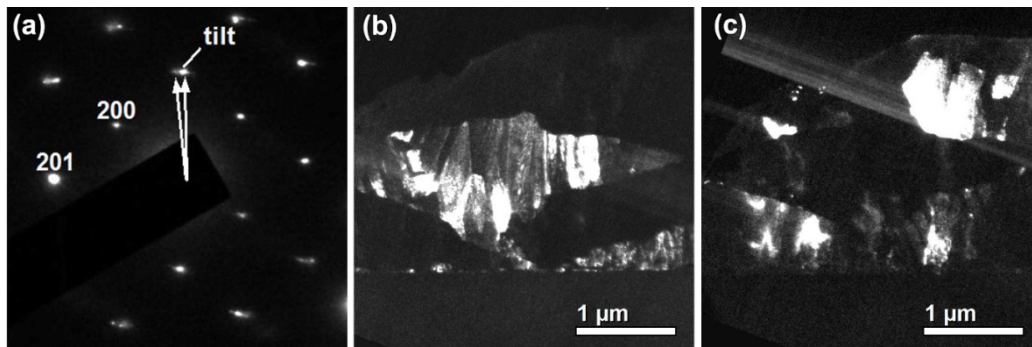

Fig. 6. A domain tilted by small angle. (a) Electron diffraction pattern showing presence of a tilt in the structure. (b) Dark-filed image obtained in a part of a diffraction streak showing the tilted domain in the layer. (c) Dark-field image showing the rest of the layer.

The new type of plane defect – stacking fault in (111) plane – is interesting from the point of view of $(Al_xGa_{1-x})_2O_3$ structural properties. Additionally, peculiarities of the twin boundaries in the case of (100) twins are important for understanding of the structural and mechanical properties of gallium oxide layers grown on sapphire substrates. These findings point that the initial stages of the growth are crucial for the obtaining of the layers with predefined crystalline quality and the corresponding studies are essential for the technology development of gallium oxide based semiconductor devices.

References
[1] J. Ahman, G. Svensson, J. Albertsson // *Acta Crystallographica Section C* **52** (1996) 1336.
[2] J.H. Kim, K.H. Yoon // *Journal of the Korean Physical Society* **53** (2008) 818.
[3] T. Miyata, T. Nakatani. T. Minami // *Journal of Luminescence* **87** (2000) 1183.
[4] Y. Tokida, S. Adachi // *ECS Journal of Solid State Science and Technology* **3** (2014) R100.
[5] D. Inomata, K. Aoki // *Proceedings of SPIE* **8987** (2014) 89871U.
[6] K. Sasaki, M. Higashiwaki, A. Kuramata, T. Masui, S. Yamakoshi // *IEEE Electron Device Letters* **34** (2013) 493.
[7] T. Oishi, Y. Koga, K. Harada, M. Kasu // *Applied Physics Express* **8** (2015) 031101.
[8] M.A. Rozhkov, E.S. Kolodeznyi, A.M. Smirnov, V.E. Bougrov, A.E. Romanov // *Materials Physics and Mechanics* **24** (2015) 194.
[9] I. Lopez, E. Nogales, P. Hidalgo, B. Mendez, J. Piqueras // *Physica Status Solidi A* **209** (2012) 113.
[10] S. Nakagomi, K. Yokoyama, Y. Kokubun // *Journal of Sensors and Sensor Systems* **3** (2014) 231.
[11] M. Fleischer, L. Hollbauer, E. Born, H. Meixner // *Journal of the American Ceramic Society* **80(8)** (1997) 2121.
[12] S.P. Arnold, S.M. Prokes, F.K. Perkins, M.E. Zaghloul // *Applied Physics Letters* **95** (2009) 103102.
[13] B. Zheng, W. Hua, Y. Yue, Z. Gao// *Journal of Catalysis* **232** (2005) 143.

[14] Y. Hou, L. Wu, X. Wang, Z. Ding, Z. Li, X. Fu // *Journal of Catalysis* **250** (2007) 12.

[15] N.K. Shrestha, K. Lee, R. Kirchgeorg, R. Hahn, P. Schmuki // *Electrochemistry Communications* **35** (2013) 112.

[16] B.J. Baliga // *Journal of Applied Physics* **53** (1982) 1759.

[17] M. Higashiwaki, K. Sasaki, A. Kuramata, T. Masui, S. Yamakoshi // *Physica Status Solidi A* **1** (2014) 21.

[18] S.I. Stepanov, V.I. Nikolaev, V.E. Bougrov, A.E. Romanov // *Reviews of Advanced Materials Science* **44** (2016) 63.

[19] S. Kumar, R. Singh // *Physica Status Solidi RRL* **7** (2013) 781.

[20] H. Frenzel, A. Lajn, M. Grundmann // *Physica Status Solidi RRL* **7** (2013) 605.

[21] H. Peelaers, C.G. Van de Walle // *Physica Status Solidi B* **252** (2015) 828.

[22] S.Y. Lee, H.C. Kang // *Journal of Crystal Growth* **412** (2015) 25.

[23] M. Mitome, S. Kohiki, K. Hori, M. Fukuta, Y. Bando // *Journal of Crystal Growth* **286** (2006) 240.

[24] S.-C. Zhu, S.-H. Guan, Z.-P. Liu // *Physical Chemistry Chemical Physics* **18** (2016) 18563.

[25] M. Baldini, M. Albrecht, D. Gogova, R. Schewski, G. Wagner // *Semiconductor Science and Technology* **30** (2015) 024013.

[26] H.W. Kim, S.H. Shim // *Thin Solid Films* **515** (2007) 5158.

[27] G. Wagner, M. Baldini, D. Gogova, M. Schmidbauer, R. Shewski, M. Albrecht, Z. Galazka, D. Klimm, R. Fornari // *Physica Status Solidi A* **211** (2014) 27-33.

[28] K. Nakai, T. Nagai, K. Noami, T. Futagi // *Japanese Journal of Applied Physics* **54** (2015) 051103.

[29] H.-S. Chung, S.C. Kim, D.H. Kim, J.W. Kim, O-J. Kwon, C. Park, H.H. Oh // *Journal of the Korean Physical Society* **55** (2009) 68.

[30] V.I. Nikolaev, A.I. Pechnikov, S.I. Stepanov, I.P. Nikitina, A.N. Smirnov, A.V. Chikiryaka, S.S. Sharofidinov, V.E. Bougrov, A.E. Romanov // *Materials Science in Semiconductor Processing* **47** (2016) 16.

[31] V.I. Nikolaev, A.I. Pechnikov, S.I. Stepanov, S.S. Sharofidinov, A.A. Golovatenko, I.P. Nikitina, A.N. Smirnov, V.E. Bugrov, A.E. Romanov, P.N. Brunkov, D.A. Kirilenko // *Semiconductors* **50** (2016) 980.